Investigating the Causes of Shear-Thinning in Non-Colloidal Suspensions: Experiments and simulations

Adolfo Vzquez-Quesada , Arif Mahmud , Shaocong Dai , Marco Ellero , Roger I. Tanner

PII: S0377-0257(17)30117-9
DOI: 10.1016/j.jnnfm.2017.08.005
Reference: JNNFM 3919

To appear in: *Journal of Non-Newtonian Fluid Mechanics*

Received date: 11 March 2017
Revised date: 15 August 2017
Accepted date: 17 August 2017

Please cite this article as: Adolfo Vzquez-Quesada , Arif Mahmud , Shaocong Dai , Marco Ellero , Roger I. Tanner , Investigating the Causes of Shear-Thinning in Non-Colloidal Suspensions: Experiments and simulations, *Journal of Non-Newtonian Fluid Mechanics* (2017), doi: 10.1016/j.jnnfm.2017.08.005

Highlights

- We study shear-thinning in non-colloidal near-Newtonian suspensions.
- Experiments and SPH simulation both show effective thinning.
- A cause is the downturn of matrix viscosity at high shear rates.
- Variable friction coefficients may also co-exist with this cause.
- Experiments are prone to edge fracture with suspensions.

Investigating the Causes of Shear-Thinning in Non-Colloidal Suspensions: experiments and simulations.

Adolfo Vázquez-Quesada[2], Arif Mahmud[1], Shaocong Dai[1], Marco Ellero[2], Roger I. Tanner[1*]

[1] School of Aerospace, Mechanical and Mechatronic Engineering, University of Sydney, Sydney 2006 Australia.
[2] Zienkiewicz Centre for Computational Engineering (ZCCE), Swansea University, Bay Campus, Swansea SA1 8EN, United Kingdom.

15/8/2017

Abstract

Experiments and computations were carried out to explore the origins of shear-thinning in non-colloidal suspensions. Two grades of polydimethylsiloxane (silicone oil) and a glycerine/water mixture were used as matrices for the suspensions. The particles were 40μm diameter polystyrene (PS) and polymethyl methacrylate (PMMA) spheres. We concentrated on 40% volume fraction suspensions where shear-thinning was clear. The silicone oil matrices were nearly Newtonian: at 24^o C the viscosity of the 1.15Pa-s sample showed a 2% drop in viscosity a shear rate of about 3000s^{-1}, the 13.2 Pa-s sample showed a drop of 2% at a shear rate of approximately 100s^{-1}, and the glycerine/water sample appeared to be Newtonian at least up to 10^4 s^{-1}. Mild shear-thinning was seen with all suspensions, beginning at shear rates of order 0.1-1 s^{-1}, followed by a rapid reduction of torque in the parallel-plate system at shear rates of 14, 150 and 1000s^{-1} respectively with the three matrices. These rapid reductions are ascribed to edge effects.

Matching smoothed particle hydrodynamics (SPH) simulations were made. The silicone matrix viscosities were modelled by a Carreau-Yasuda (CY) fit up to shear rates of order 10^7 s^{-1}. The agreement between computations and experiments is generally good for 40% volume fraction suspensions up to the shear rate where edge effects intervene in the experiments- there are no edge effects in the simulations. This confirms the suggestion [1] by Vázquez-Quesada et al [*Phys. Rev. Lett,* **117**, 108001 (2017)] that 'hidden' high shear rates between particles, where the non-Newtonian matrix viscosity comes into play, can result in shear-thinning at the macroscopic level. For the glycerine/water matrix at low shear rates this mechanism does not apply and a separate mechanism based on variable interparticle friction is suggested; the two mechanisms can co-exist.

A.Introduction

Non-colloidal suspensions of spheres with Newtonian matrices at negligible Reynolds numbers would be expected to show a viscosity (η) that is a multiple of the matrix viscosity (η_o) and a relative viscosity ($\eta_r = \eta/\eta_o$) which is a function only of the volume fraction of the spheres (ϕ). However, from experiments [2, 3] one sees that shear thinning does occur when $\phi \geq 0.3$ and the cause is not clear. There is one possible explanation [4, 5] that depends on

variation of the interparticle friction coefficient with shear rate. A second explanation has been made [1] which depends on the matrix being shear-thinning at the enhanced shear rate between the particles; at the macroscopic or mean shear rate the matrix fluid has a constant viscosity.

This mechanism should not be confused with various investigations where the matrix is highly shear-thinning near the region of the mean shear rate. For example in [6] power-law matrices were assumed, while in other cases [7, 8] estimates of shear rate amplification are given. For 40% volume fraction suspensions strain-rate amplifications of about 4 [7] to 8 [8] were reported. We note the investigations of Liard et al [9], which will be discussed later in Section E. In all these cases the result is a shifted viscosity-shear rate curve which has a form similar to the matrix viscosity curve. However, in the investigation by Vázquez-Quesada et al [1] and in the present paper the resulting viscosity curve is not of the same form as the assumed matrix relation because of the complex probability distribution of the actual shear rates in the suspensions. Hence it differs from the quasi-static picture in the cited references [7-9]. The earlier smoothed particle hydrodynamics (SPH) investigation [1] contained a rough power-law matrix viscosity rule; in the present paper a much more realistic model is used.

From the earlier SPH simulations [1] it was suggested that there were regions of very high shear rate between the spherical particles in which shear thinning of the matrix took place; this local shear thinning of the matrix at high shear rates leads to shear thinning at the average (macroscopic) shear rate. Since the matrix shear-thinning is negligible at the mean shear rate and the local thinning occurs well beyond the mean shear rate it was therefore termed a 'hidden' mechanism.

The primary aim of the present paper is to compare some typical experimental results with the second explanation. It should be mentioned that the ratio of viscous forces to Brownian forces (the Péclet number,P_e) in the suspensions was always of order 10^8, well into the non-colloidal region [5]; the Reynolds number (R_e) was also negligible. Here, $R_e = \frac{\rho \Omega R a}{\eta_0}$, where ρ is the fluid density, ΩR is the rim speed in the viscometer, and a is the sphere radius. Typically, even at a high shear rate of $100s^{-1}$, R_e was of order 10^{-2}, which is small.

Our work therefore seeks to explore shear thinning in non-colloidal suspensions. We experimented with two different matrix materials (silicone oil and glycerine/water) and two spherical bead materials. Polymethyl methacrylate (PMMA) beads were used in the glycerine/water matrix and polystyrene (PS) beads were used in silicone oil in order to minimize density differences between beads and matrices.

For colloidal suspensions, where Brownian motion is relevant, reasonable predictions of the suspension rheology exist, and shear thinning is observed as result of a decreasing relative contribution of entropic forces at large shear rates [10]. However, no such mechanism is present in non-colloidal suspensions.

B. Experimental Procedure.

Table 1. Matrix fluid properties.

Matrix	Density, ρ (kg/m^3)	Viscosity, η_o (Pa-s)	$N_1/\dot{\gamma}^2$ ($Pa\text{-}s^{2)}$)	λ (s)
1000cs Silicone oil	970	1.15	$2.3x10^{-4}$	$1x\ 10^{-4}$
12500cs Silicone oil	973	13.2	0.029	0.0012
Glycerine/water mix	1249	0.606	-	-

All the experiments were performed with a Paar Physica MCR 300 rheometer at a constant temperature of 24°C. We used silicone oils of different viscosity as matrices, see Table 1. The grades used were nominal 1000cs and 12500cs. formations. The density of silicone oils were 970 kg/m^3 and 973kg/m^3 respectively and that of polystyrene (PS) was 1050 kg/m^3. The mean diameter of the polystyrene beads was 40.88μm with a standard deviation of 2.75μm [5]. The glycerine/water suspensions used PMMA beads of mean diameter 40.45μm with a standard deviation of 3.89μm. The densities of the glycerine/water and the PMMA were 1249 kg/m^3 and 1160 kg/m^3 respectively.

We used a 50mm diameter cone-plate system (CP50-1) for the silicone oils with a vertex gap of 0.05mm. 50mm parallel plates (PP50) were used to measure the viscosity of the silicone-based suspensions; the gap was 1mm. We used the same rheometer with PP50 parallel plates to investigate the viscosity of the glycerine/water matrices and the 40%PMMA-glycerine/water suspensions. The gaps in this case were 0.1mm for the matrix fluid and 0.5mm for the suspensions.

C. Matrix Properties

The observed low shear rate viscosities were 1.15 Pa- s for 1000cs silicone and 13.2 Pa.-s for 12500cs silicone at the temperature of 24°C (Fig.1). Hence the 12500cs silicone oil has 11.5 times higher viscosity than the 1000cs silicone oil at the same shear rate (0.1 s^{-1}). The results for the glycerine/water (2% water) matrix are shown in Fig. 2.

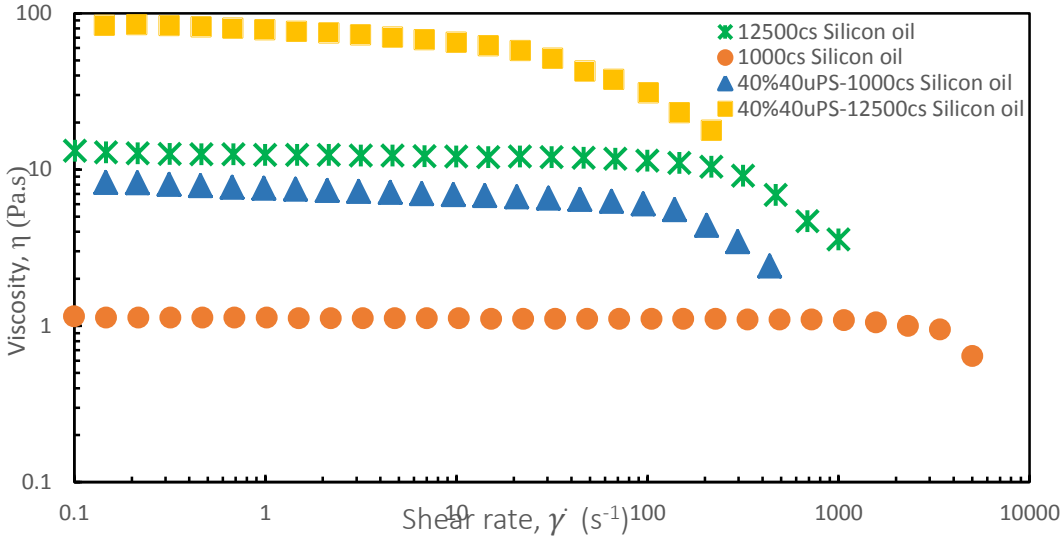

Fig. 1 Effects of shear rate in silicone matrices (12500cs silicone oil (x) and 1000cs silicone oil (●) and 40% volume fraction PS-Silicone (12500cs silicone (■) and 1000cs silicone (▲)) suspensions at a constant temperature of 24°C. The PS beads were 40μm in diameter. Note that the shear thinning of the suspensions extends down to shear rates of order $0.1s^{-1}$.

In Fig.1, circles and stars represent 1000cs silicone oil and 12500cs silicone oil results respectively. Both of them apparently show almost no change in viscosity with the increase of shear rate up to a critical value, indicating Newtonian flow of the matrix up to this point. However, one should not necessarily attribute the sudden downturn of viscosity of the silicones to shear thinning.

We can see, from Table 1 that silicone oils exhibit normal stresses, and hence they are slightly viscoelastic. From measurements of the first normal stress difference (N_1) using the cone-plate system one can define a relaxation time (λ) from:

$$N_1 = 2\eta_o \lambda \dot{\gamma}^2 \qquad (1)$$

where $\dot{\gamma}$ is the macroscopic shear rate. One expects shear-thinning to occur if the Weissenberg number (*Wi)*, defined as $\lambda\dot{\gamma}$, is of order 1 or greater. Table 2 shows the expected shear rate ($\frac{1}{\lambda}$) at which shear-thinning is expected to commence and the observed critical shear rate ($\dot{\gamma}_c$).

The observed rates for a 10% downturn of torque ($\dot{\gamma}_c$) are found from Fig 1 for the silicone fluids to be about 3000 and $200s^{-1}$ and for the glycerine/water fluids (Fig 2) to be greater than 10^4 s^{-1} (Table 2). Hence it appears that for silicone oils $\dot{\gamma}_c < \frac{1}{\lambda}$, and it is possible that the observed downturn with the silicones is due to edge fracture [11]. We can estimate the rate at which edge fracture occurs ($\dot{\gamma}_e$) as follows, using the work of Keentok and Xue [11]. According to [11], edge fracture occurs in cone/plate and parallel-plate rheometers when

$$N_{2c} = 2\,\sigma_s/3b \qquad (2)$$

where N_{2c} is the critical second normal stress difference magnitude at the rim shear rate and σ_s is the surface tension coefficient (0.021 Pa-m for silicones). If h is the gap at the rheometer edge, then the 'flaw' size b = 0.12h. From Eq. 2, where h =1mm, we find N_{2c} = 114 Pa. From [3] $-N_2 / N_1$ is small for the 1000cs silicone, and it lies between 0.07 and 0.1 for the 12500cs silicone [12]. Using 0.07-0.1 for the ratio for the 12500cs fluid we estimate that edge fracture occurs for $\dot{\gamma}_e \sim 198\text{-}240 s^{-1}$ as shown in Table 2, which is in reasonable agreement with Fig 1.
The glycerine/water matrix was not observed to fracture at the edge, at least up to a shear rate of 10^4 s^{-1}. For the glycerine/water mix, the slight downturn of viscosity at the largest shear rates may be due to shear heating. From [13] we find the rise in temperature (ΔT) at the central plane in a shear flow is $\eta_o \dot{\gamma}^2 h^2 / 8\kappa$, where κ is the thermal conductivity and h and $\dot{\gamma}^2$ are values at the rim. For glycerine $\kappa \sim 0.28$ W/mK. This gives, at a rim shear rate of 10^4 s^{-1} and h=0.1mm, a maximum temperature rises of about 0.5°C. According to Kaye and Laby [14] a 98% glycerine /2% water mix at 25° C changes its viscosity by about 8% per ° C. Hence a drop of viscosity of about 4% maximum is expected at a rim shear rate of 10^4 s^{-1}; Fig. 2 shows a change of about 3%. Hence we believe this matrix is Newtonian up to at least a rim shear rate of 10^4 s^{-1}.

Table 2. Critical shear rates.

Matrix	$(\frac{1}{\lambda})$ s^{-1}	Observed $(\dot{\gamma}_c)$ s^{-1}	Edge rate $(\dot{\gamma}_e)$ s^{-1}
1000cs silicone	10^4	3000	-
12500cs silicone	833	200	198-240
Glycerine/water	$>> 10^4$	$> 10^4$	Large

To explore the suggestion [1] that high interparticle shear rates influence suspension behaviour with matrices that are apparently Newtonian, it is necessary to know the matrix viscosities at shear rates of order 10^6 s^{-1} or larger. We refer to the work of Swallow [15] and Barlow *et. al.* [16]. Swallow [15] suggested that the Cox-Merz [17] rule held for silicones. Barlow *et. al.* [16] did extensive high-frequency tests on silicones, measuring G' and G" from 10^4 to 10^8 Hz. Using the Cox-Merz relation we have, approximately

$$\eta(\dot{\gamma}) \sim \eta^*(\omega) = \frac{\sqrt{(G'^2 + G''^2)}}{\omega} \qquad (3)$$

where, ω is the frequency of oscillation (rad/s; $\omega = 2\pi f$; f in Hz).

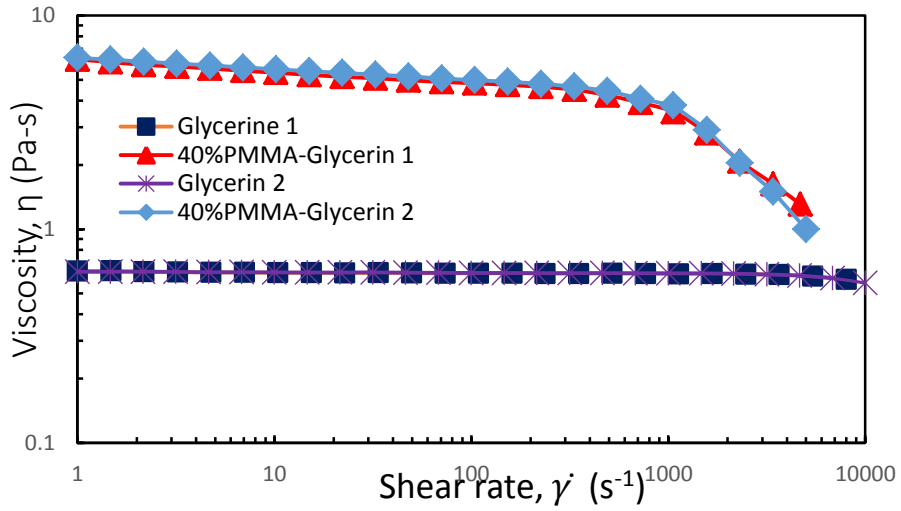

Fig. 2 Effects of shear rate in glycerine/water matrix and 40% volume fraction PMMA-Glycerine suspension at a constant temperature of 24°C. Glycerine 1 and 2 are duplicate tests of the same material.

The results of Barlow et al [16] are normalized to 30° C, and hence there is a change for other temperatures; we used 24°C in all tests. There are also slightly larger viscosities with our silicone samples-13.2 Pa-s and 1.15 Pa-s, whereas Barlow et al report 12.3 and 1.01 Pa-s.

The variation of viscosity with temperature obeys the equation [18]

$$\log_{10}\left[\frac{\eta_{T°C}}{\eta_{30°C}}\right] = \frac{-C_1(T-30)}{C_2+(T-30)} \qquad (4)$$

Table 3. Comparison between Barlow et. al. data [16] with our experimental data.

Viscosity grade(cs)	Viscosity, η (Pa-s) at 30°C	Viscosity, η (Pa-s) at 24°C	Viscosity, η (Pa-s) at 24°C Experimental	Percentage of difference in viscosity, η (Pa-s)	Density, ρ (kg/m^3) at 30°C	Density, ρ (kg/m^3) at 24°C	Density,ρ (kg/m^3)at 24°C Experimental
1000cs	0.896	1.012	1.15	12%	965	970	970
12500cs	10.85	12.25	13.2	7.19%	968	973	973

Equation (4) was used to obtain extrapolated values of viscosity at the lower temperature, where the values of C_1=1.90 and C_2=222 °C were assumed.

The variation of density with temperature was found to be described satisfactorily by the equation,

$$\frac{1}{\rho_{T°C}} = \frac{1}{\rho_{30°C}}[1 + C_3(T-30)] \qquad (5)$$

where, the values of C_3 were 8.53×10^{-4} °C^{-1}, 8.84×10^{-4} °C^{-1}, 8.60×10^{-4} °C^{-1} for the 1000cs and 12500cs samples respectively.

The results of taking the G' and G" data of [16] and finding the value of the shear viscosity using Eq. 3 and the relation $\eta^*(\omega) = \eta(\dot{\gamma})$ are shown in Table 4; the reduction of viscosity is clear.

Table 4. η^* as a function of shear rate from the data in [16] at 24° C.

$\dot{\gamma}$,ω (s^{-1})	η^* Pa-s; 1000cs	η^* Pa-s; 12500cs
5.564×10^4	0.706	1.69
5.564×10^5	0.265	0.356
5.564×10^6	0.070	0.086

We plot these results in Fig. 3, noting that the analysis of Vázquez-Quesada et al [1] used a viscosity rule:

$$\frac{\eta}{\eta_0} = \begin{cases} 1, & \text{if } \dot{\gamma} < \dot{\gamma}_c \\ \left(\dot{\gamma} / \dot{\gamma}_c\right)^{-m}, & \dot{\gamma} > \dot{\gamma}_c \end{cases} \qquad (6)$$

From Fig. 3 we find m = 0.43 for the 1000cs sample, and m = 0.70 for the 12500cs sample. The values of the critical shear rates where the horizontal lines intersect the power-law lines are about 2.4×10^4 s^{-1} and 3.16×10^3 s^{-1} respectively. From the normal stress data (Table 2) the comparable critical rates were 10^4 s^{-1} and $833 s^{-1}$ respectively. Hence it is clear that the silicone matrices are Newtonian up to shear rates around 10^4 s^{-1} and 10^3 s^{-1} respectively, and then they obey power-laws after a short transition, which is not captured in Fig 3.

Further data are shown by Lee [19], but the most useful data come from the Dow-Corning website [20]. There it is seen that the 1000cs and 12500cs grades show a reduction of viscosity at shear rates of 10^4 and 10^3 s^{-1} respectively.

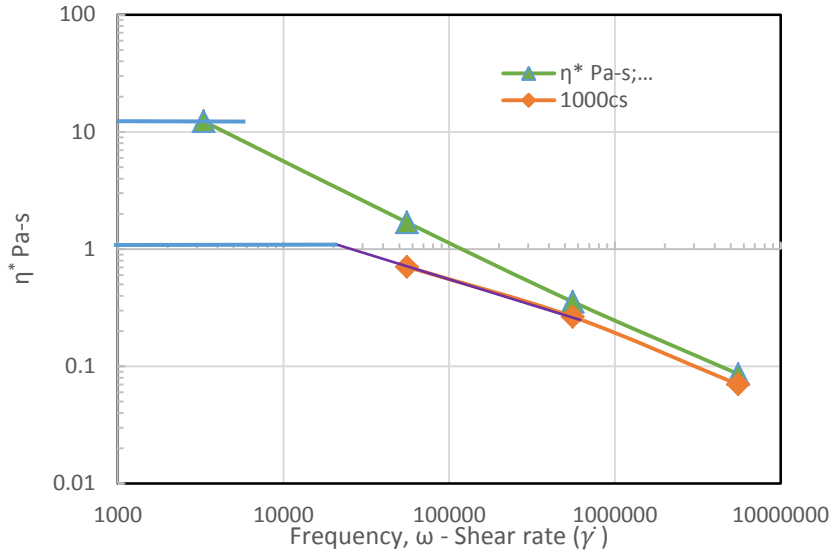

Fig.3 Showing the high-frequency shear data [16] and the power-law behaviour for the two silicone fluids.

The matrix behaviour for both silicones is shown in Fig 4. Whilst the power-law model (Eq 6) was used previously [1], a much better fit to the data is given by the Carreau-Yasuda (CY) model [21], and this has been used in the subsequent computations reported here. One sees from Fig 4 that the cone-plate data for the silicone matrix experiments (symbol □) diverge from the other data at comparatively low shear rates. This is due to edge effects in the cone-plate system; it is necessary to use capillary or oscillatory data to avoid this effect.
For glycerine we can refer to a paper by Barlow and Lamb [22] who found that the limiting elastic modulus (G_m) at high frequency was 2.3 x10^9 Pa. Hence a relaxation time $\eta_o/G_m \sim 2.6 \times 10^{-10}$ s is expected for this matrix and no observable shear-thinning in the rheometer is expected.

D. Suspension Response

The 40%PMMA-glycerine/water suspensions exhibit shear-thinning (Fig. 2). The viscosity falls steadily but quite slowly up to a shear rate of 1060 s^{-1}, but with an increase of shear rate above 1060 s^{-1}, the viscosity apparently decreases rapidly.

For the silicone oil suspensions, the square and triangle marked lines in Fig 1 refer to the 40% volume fraction PS-12500cs and PS-1000cs suspensions. At a shear rate of 0.1s^{-1} the viscosity of the 12500cs silicone suspension has increased to 77.5 Pa-s from the viscosity of the matrix of 13.2 Pa-s; the viscosity of the PS-1000cs suspension was 6.37 times higher than the viscosity of the 1000cs silicone matrix.

The viscosity of the 12500cs silicone suspension appears to fall quickly from 57.8 Pa-s at a shear rate of 31.9 s^{-1}. The viscosity of the 1000cs silicone suspension appears to fall rapidly at a shear rate of 204 s^{-1}. These sharp declines are believed to be due to edge fracture [11,13].

Shear-thinning appears to begin at very low shear rates (~ 0.1s^{-1}). The slopes of the viscosity-shear-rate curves are not large here; in all cases the slope is of order -0.05 on the logarithmic plots. For the sharp declines at larger shear rates, we consider edge effects. Edge effects, following Eq. 2, depend on the second normal stress difference N_2. Suspensions with Newtonian matrices have a second normal stress difference given by [3]

$$N_2 = -4.4\eta\,\dot{\gamma}\phi^3 \qquad (7)$$

and for ϕ=0.4, the magnitude of N_2 is 0.28 $\eta\,\dot{\gamma}$.
The fracture criterion (2) was developed on the basis of a second-order fluid model [13] and it is not clear that the factor b = 0.12h in Eq (2) is appropriate for suspensions. For the suspensions it seems likely that a more appropriate length scale for b is not h but something of the order of the sphere radius (a) . Replacing 0.12h by 30μm (1,5 times the sphere radii) gives the following results.

For the 1000cs suspensions, Eq 2 now predicts a critical shear rate due to edge fracture of ~ 150s^{-1}; for the 12500cs suspension, the onset of edge effects is expected at a shear rate of about 13s^{-1}, and for the glycerine/water suspensions, edge effects are expected to appear at a shear rate exceeding 550s^{-1}. These results match the results in Figs 1 and 2 quite well.

E. Numerical results

In this section, results from simulations (using the SPH model described in the Appendix) and experiments will be compared. To do the comparison, the rheology of the solvent has to be well characterized. Both matrices considered here, Dow-Corning silicone 1000cs and 12500cs can be very well characterized using the Carreau-Yasuda (CY) model [21]

$$\frac{(\eta-\eta_\infty)}{(\eta_0-\eta_\infty)} = \left(1+\left(\lambda\dot{\gamma}\right)^A\right)^{(m-1)/A} \qquad (8)$$

where η_0 and η_∞ are the limiting viscosities at low and high shear rates respectively, $\dot{\gamma}_c = 1/\lambda$ determines the transitional shear rate between the extreme viscosities, A determines the width of the transition and m is the power law exponent of the viscosity decay within the transition.

Both matrix fluids, 1000cs and 12500cs, can be reproduced fairly well with similar parameters for the CY model but with different relaxation times. The parameters used for both silicone characterizations were $\eta_\infty = 0$, $A = 1.2$ and m-1 = -0.55. The relaxation times, however, are taken as $\lambda = 3.10^{-5}$ s for the silicone 1000cs, and as $\lambda = 7.10^{-4}$ s for the silicone

12500cs. In Fig. 4 both characterizations have been drawn and compared to previous rheological data as well as data reported by the manufacturer Dow Corning [16, 19, 20], and those corresponding to this work, showing an excellent fit, especially to the Dow-Corning data[20]. As mentioned above in Section C and Fig 4, the divergence of our cone-plate experiments from the other data is due to edge effects; there are no edge effects in the simulations.

In the simulation setup we consider a box of size $L_x \times L_y \times L_z$, confined between two planar walls separated by a distance $L_z = 64a$, with a being the radius of the solid particles. The walls move with velocities $\pm V^w$ in the x direction to generate a shear rate $\dot{\gamma}$ in the plane x-z. Note that the effective shear rate $\dot{\gamma}$ measured in the bulk is, in general, slightly smaller than the imposed one $\dot{\gamma}^{in} = 2V^w / L_z$. In the following rheological analysis we always measure the bulk $\dot{\gamma}$ to avoid possible artefacts due to small amount of wall slip. The size of the box is $L_x = 16a, L_y = 8a$ and $L_z = 64a$, selected large enough to rule out possible confinement as well as finite size effects. Once the steady state is reached, the viscosity can be calculated from averaging of the tangential force acting on the wall as $\eta_{susp} = F_x / \left(L_x L_y \dot{\gamma} \right)$. In order to compare the rheology of the simulated particulate system with the experimental results shown in Sec. D, a dimensionless shear rate is defined as $\dot{\gamma}^* = \dot{\gamma} / \dot{\gamma}_c = \dot{\gamma}\lambda$ where λ are the relaxation times for the different silicon matrices obtained by fitting their rheology using the CY model discussed above. In simulations, the shear rate is kept fixed at $\dot{\gamma} \approx 0.013$ so that the particle Reynolds number $R_e = \rho a^2 \dot{\gamma} / \eta \approx 0.0016$ remains constant and small. In order to span the same regime of dimensionless shear rates observed in experiment ($\dot{\gamma}^*$~[10^{-5}-10^{-1}]), the parameter $\dot{\gamma}_c$ (defining the viscosity model Eq.(8) entering the lubrication Eq.(12): see Appendix) is changed in the simulation.

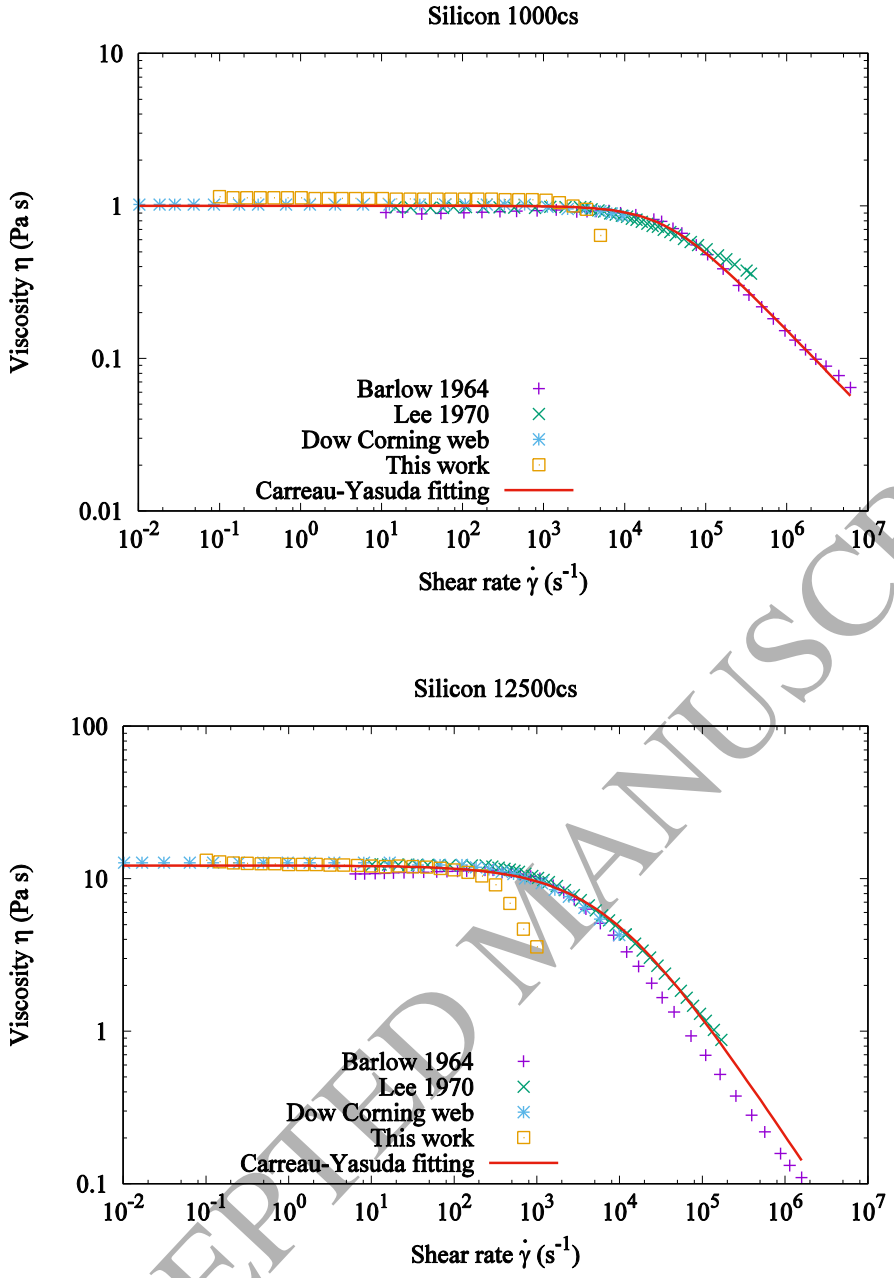

Fig.4 Characterization of the solvent rheology with the CY model for silicone 1000cs and silicone 12500cs compared with previous results [16, 19, 20] and with our experiments [□].

In Fig. 5 the comparison of the relative suspension viscosity obtained from simulations and experiments is shown. Silicone 1000cs and 12500cs matrices are considered and the dispersed solid phase is at a concentration $\phi = 0.4$.

Good agreement of the shear thinning decay and the value of the viscosity is obtained in both cases in the range of dimensionless shear rate $\dot{\gamma}^*$~[10^{-4}-10^{-2}]. Note that no additional fitting parameters have been used other than those used to fit the data in Fig 4, and the computed response is not a shifted version of the Carreau-Yasuda model.

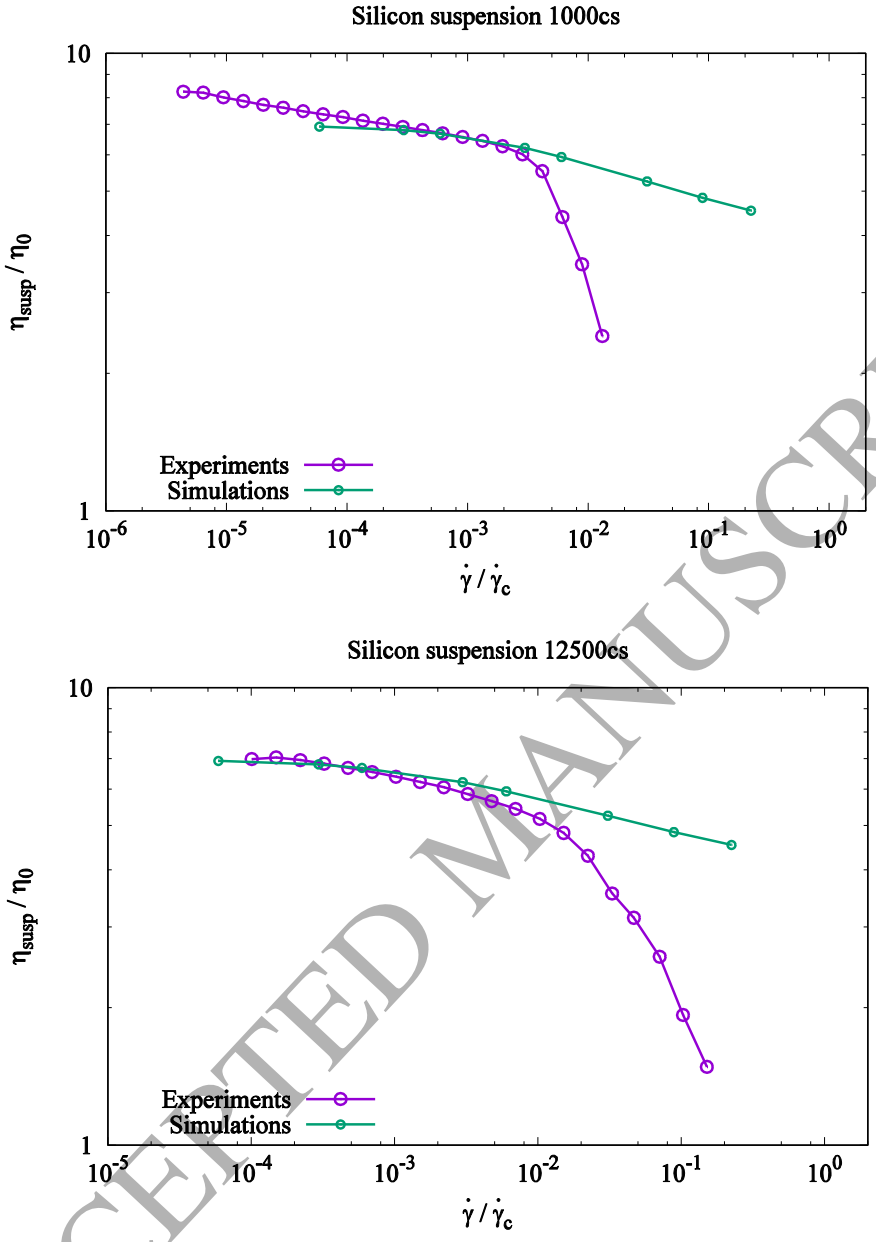

Fig 5. Rheology of 40% suspensions. Comparison of the simulations with the experimental results with the silicone matrices

In simulations, however, the power law viscosity decay extends to higher shear rates compared to the experiments, i.e. towards values approaching $\dot{\gamma}_c$ for the respective matrices. On the contrary, experimental results show a sudden downturn in the viscosity well below the estimated $\dot{\gamma}_c$ (starting approximately at $\dot{\gamma}^* \sim 10^{-2}$). This discrepancy is due to second normal stress differences causing edge fracture; note that the second normal stress difference is much enhanced in suspensions (Eq. (7)).

As a result, it is expected that suspensions with silicone matrices exhibiting the rheology shown in the Fig. 4 and without edge fracture problems, will show extended power-law viscosity decrease without sudden downturn effects.

It should be noticed that a similar numerical approach was used in [9] to explore the effects of the matrix shear-thinning on the suspension. In that work, however, the authors focused on a regime of bulk shear rates in the same order of the matrix $\dot{\gamma}_c$ (i.e. $\dot{\gamma}^*$~10^{-1}-10^{2} in our notation). In agreement with previous literature, they observe a scaling regime in that range of shear rates which allows one to predict suspension bulk rheology based on matrix properties alone. We point out that in the low shear rate regime explored in this work (i.e. $\dot{\gamma}^*$~10^{-4}-10^{-1}), mild shear-thinning of the suspension cannot be directly linked to the matrix shear-thinning, in fact the scaling exponents are different in the two cases. We believe that in this regime the suspension viscosity derives from a complex interplay between matrix property and changing anisotropic microstructure. This, on the other hand, is consistent with the results presented in [9] (see their Fig. 3-4) where experimental data for the suspension viscosity collapse poorly on a master curve at large concentrations and small shear rates. This was also proved by their scaling error (see their Fig-4) which shows values as high as 10% at concentration $\phi = 0.4$. Remarkably, that change in relative viscosity reported is precisely the difference in the computed bulk viscosity (shear thinning) that we observe at low shears (see Fig. 5), so our results here can explain the failure in the scaling proposed in [9] in the low shear rate regime.

Another aspect which deserves discussion is represented by the very low shear rate regime (i.e. for $\dot{\gamma}^*$<10^{-4}). It seems that, under the current conditions, our model based on the 'hidden' shear-thinning mechanism [1] is not able to reproduce the shear-thinning observed in experiments down to $\dot{\gamma}^*$~10^{-5} (see silicone 1000cs) where a plateau is observed instead. This deviation results in a smaller relative viscosity measured in simulations with respect to experimental values and suggests the possibility of additional frictional effects which are not taken into account in our 'hidden' shear rate model. Note that frictional effects should not be relevant at higher shear rates (at $\phi = 0.4$) where good quantitative agreement in the exact values of the viscosity is obtained. The results with a glycerine/water matrix do not fit the pattern of the present simulation model and therefore remain to be explained, most probably by an interparticle friction mechanism [5].

F. Conclusion

It is perhaps unexpected, following [5] and the work of Mari et al [23], that there is so close an agreement between the computed and experimental relative viscosities in Fig 5 when no explicit Coulombic friction was used in the SPH computations. It appears that at ϕ= 0.4, frictionless computations [5,23] give a relative viscosity of 6.2 ±0.4, whereas in reference [1] a Newtonian SPH computation yields a relative viscosity of 6.85 at low shear rates. Looking at Fig 6 one sees that the compound spheres are not completely smooth. In reference [5] we found that roughness increases relative viscosity, and so it appears that this suffices to explain the quite small increase of relative viscosity seen in the computations- it appears there is a 'de facto' friction coefficient in the computations of 0.1-0.2, which is actually due to the roughness ratio of about 5% [5].

It appears that the 'hidden' shear-thinning mechanism [1] must exist due to the high shear rates (relative to the macroscopic shear rate) between the particles, bringing into play the shear-thinning of the apparently 'Newtonian' matrices. The agreement between the computed relative viscosity and the experimental results in the middle range of shear rates is striking and demonstrates the importance of 'hidden' shear-thinning matrix effect in this regime. At very low shear rates the frictional effects [4,5] seem to be more important as is seen in the results with the glycerine/water matrices, where the matrix shear-thinning - possibly occurring at extremely high-shear rates - is unlikely to affect suspension rheology at very low macroscopic shear rates. This is because the simulations with a Newtonian matrix [1] do not show shear-thinning, whereas it is clearly seen in the experimental data in Fig 2.The two mechanisms can clearly co-exist. In addition, the problem of edge fracture is always present in parallel-plate and cone-plate experiments with suspensions and can seriously interfere with the interpretation of the phenomena, so care is needed.

G. Acknowledgements

We thank the University of Sydney for providing scholarship support for Arif Mahmud. Adolfo Vázquez-Quesada and Marco Ellero gratefully acknowledge the financial support provided by the Welsh Government and Higher Education Funding Council for Wales through the Ser Cymru National Research Network in Advanced Engineering and Materials. Computing resources offered by HPC Wales via the project Nr. HPCWT050 (Multiscale particle simulation for complex fluids) are also gratefully acknowledged. Adolfo Vázquez-Quesada also thanks MINECO (Spain) for support under Grant No. FIS2013-47350-C5-1-R.

References

[1] Vázquez-Quesada, A., Tanner, R. I. & Ellero, M. (2016). Shear Thinning of Noncolloidal Suspensions. *Physical Review Letters, 117*, 108001-108005.

[2] Zarraga, I. E., Hill, D. A., & Leighton Jr, D. T. (2000). The characterization of the total stress of concentrated suspensions of non-colloidal spheres in Newtonian fluids. *Journal of Rheology*, *44*, 185-220.

[3] Dai, S. C., Bertevas, E., Qi, F. Z., & Tanner, R. I. (2013). Viscometric functions for noncolloidal sphere suspensions with Newtonian matrices. *Journal of Rheology*, *57*(2), 493-510.

[4] Cates, M. E., & M. Wyart (2014). Granulation and bistability in non-Brownian suspensions. *Rheol. Acta*, *53*, 755–764.

[5] Tanner, R. I., & Dai, S. (2016). Particle roughness and rheology in noncolloidal suspensions. *Journal of Rheology*, *60*(4), 809-818.

[6] Tanner,R.I., Qi,F.,& Housiadas, K.D (2010). A differential approach to suspensions

with power-law matrices. , *Journal of Non-Newtonian Fluid Mechanics 165*, 1677-1681.

[7] Chateau,X.,Ovarlez,G.,Trung, K.L.(2008). Homogenization approach to the behaviour of suspensions of noncolloidal particles in yield stress fluids. *Journal of Rheology, 52*, 489-506.

[8] Tanner,R.I.& Dai, S.C (2016) Rheology of non-colloidal suspensions with corn syrup matrices. *Rheologica Acta 55*, 739-747.

[9] Liard,M., Martys,N.S. George,W.L., Lootens,D. & Hebraud ,P.(2014). Scaling laws for the flow of generalized Newtonian suspensions. *Journal of Rheology* 58, 1993-2015.

[10] Mewis, J. & Wagner, N. J. (2011). *Colloidal Suspension Rheology* (Cambridge University Press, Cambridge), Cambridge Books Online.

[11] Keentok, M. and S.-C. Xue (1999). "Edge fracture in cone-plate and parallel plate flows." *Rheologica Acta 38*(4), 321-348.

[12] Mall-Gleissle, S. E., Gleissle, W., McKinley, G. H., & Buggisch, H. (2002). The normal stress behaviour of suspensions with viscoelastic matrix fluids. *Rheologica acta*, *41*(1-2), 61-76.

[13] Tanner, R. I. (2000). Engineering Rheology, 2nd ed. (Oxford University Press, Oxford).

[14] Kaye, G. W. C. and Laby, T. H. (1914). Physical and chemical constants and some mathematical functions . 11th ed,. Longmans, Green and Co, London.

[15] Swallow, F.E. (2002).Viscosity of polydimethylsiloxane gum: Shear and temperature dependence from dynamic and capillary rheometry. *J. Appl. Polymer Sci., 84*, 2533-2540.

[16] Barlow, A.J., Harrison, G., Lamb, J. (1964). Viscoelastic relaxation of polydimethylsiloxane liquids. *Proc. Roy. Soc. London, A282*, 228-251.

[17] Cox, W.P., Merz, E.H. (1958). Correlation of dynamic and steady flow viscosities. *J. Poly. Sci*, 28, 619-622.

[18] Williams, M. L., Landel, R. F., & Ferry, J. D. (1955). The temperature dependence of relaxation mechanisms in amorphous polymers and other glass-forming liquids. *Journal of the American Chemical society*, *77*(14), 3701-3707.

[19] Lee, C. L., Polmanteer, K. E., & King, E. G. (1970). Flow behavior of narrow-distribution polydimethylsiloxane. *Journal of Polymer Science Part A-2 :Polymer Physics*,8(11).1909-1816.

[20] http://www.dowcorning.com/content/discover/discoverchem/si-rheology.aspx

[21] Yasuda, K. Y., Armstrong, R. C. & Cohen, R. E. (1981). Shear flow properties of concentrated solutions of linear and star branched polystyrenes. *Rheologica Acta*, *20*(2), 163-178.

[22] Barlow, A.J., Lamb, J. (1959). The visco-elastic behaviour of lubricating oils under cyclic shearing stress. *Proc. Roy. Soc.London A253*, 52-79.

[23] Mari,R.,Seto,R.,Morris,J.F.,Denn,M.M.(2014). Shear thickening, frictional and frictionless rheologies in non-Brownian suspensions.*J. Rheol.58*,1693-1724.

[24] Vázquez-Quesada A., Ellero M. (2016). Rheology and microstructure of non-colloidal suspensions under shear studied with smoothed particle hydrodynamics, *Journal of Non-Newtonian Fluid Mechanics 233*, 37-47.

[25] Español P., Revenga M. (2003). Smoothed Dissipative Particle Dynamics, *Physical Review E 67* (2), 026705.

[26] Morris J. P., Fox P. J., Zhu Y.(1997). Modeling low Reynolds number incompressible flows using SPH, *Journal of Computational Physics 136* (1), 214-226.

[27] Monaghan J. J. (1994). Simulating free surface flows with SPH, *Journal of Computational Physics*, *110* (2), 399-406.

[28] Bian X., Litvinov S., Qian R., Ellero M. (2012). Multiscale modeling of particles in suspension with Smoothed Dissipative Particle Dynamics, *Physics of Fluids 24* (1), 012002.

[29] Kim S., Karrila S. J.(1991). Microhydrodynamics: principles and selected applications.

[30] Nguyen N. Q., Ladd A. (2002). Lubrication corrections for Lattice-Boltzmann simulations of particle suspensions, *Physical Review E 66* (4), 046708.

[31] Bian X., Ellero M. (2014). A splitting integration scheme for the SPH simulation of concentrated particle suspensions, *Computer Physics Communication 185* (1), 53-62.

[32] Dratler D., Schowalter W.(1996). Dynamic simulation of suspensions of non-brownian hard spheres, *Journal of Fluid Mechanics 325*, 53-77.

[33] J. F. Brady, Morris J. F.(1997). Microstructure of strongly sheared suspensions and its impact on rheology and diffusion, *Journal of Fluid Mechanics 348*, 103-139.

Appendix: Smoothed Particle Hydrodynamic model of suspension

To simulate the system, the suspension model presented in [24] has been modified. The matrix is simulated with SPH, which is a meshless Lagrangian fluid model where the Navier-Stokes equations are discretized using a set of points denoted as fluid particles. Positions and momenta of every fluid particle (labelled by Latin indices $i = 1,\ldots,N$) evolve in a Lagrangian framework, according to the SPH discrete equations

$$\dot{\mathbf{r}}_i = \mathbf{v}_i \tag{9}$$

$$m\dot{\mathbf{v}}_i = -\sum_j \left[\frac{P_i}{d_i^2} + \frac{P_j}{d_j^2}\right]\frac{\partial W(r_{ij})}{\partial r_{ij}}\mathbf{e}_{ij} + \sum_j (D+2)\eta_0\left[\frac{1}{d_i^2} + \frac{1}{d_j^2}\right]\frac{\partial W(r_{ij})}{\partial r_{ij}}\frac{\mathbf{e}_{ij}\cdot\mathbf{v}_{ij}}{r_{ij}}\mathbf{e}_{ij} \tag{10}$$

where D is the number of dimensions of the system, P_i the pressure of particle i, $\mathbf{e}_{ij} = \mathbf{r}_{ij} / r_{ij}$ the unit vector joining particles i and j, $\mathbf{v}_{ij} = \mathbf{v}_i - \mathbf{v}_j$ their velocity difference and η_0 the viscosity of the solvent. $d_i = \sum_j W\left(r_{ij}, r_{cut}\right)$ is the number density associated to particle i estimated as a weighted interpolation with a bell-shaped function W with compact support r_{cut}. With this definition, mass conservation and continuity equations for the mass density $\rho_i = m d_i$ (m particle mass) are implicitly satisfied [25]. Equation (10) is Newton's equation of motion of the particle i which is a discrete representation of the momentum Navier-Stokes equation in a Lagrangian framework. A quintic spline weighting function W [26] is used, with cutoff radius $r_{cut} = 4dx$ (dx being the mean fluid particle separation). Finally, an equation of state for pressure is chosen as $P_i = p_0\left[\left(\rho_i / \rho_0\right)^7 - 1\right] + p_b$ where the liquid speed of sound $c_s = \sqrt{7 p_0 / \rho_0}$ is taken sufficiently large to enforce incompressibility [27].

Boundaries and solid inclusions are modelled by using boundary particles similar to the fluid ones, located inside the solid regions as discussed in Ref. [28] (Fig. 6). In the case that two solid inclusions are very close, the analytical solution of the lubrication interaction between spheres [24] can be used. Both normal $\mathbf{F}^n_{\alpha\beta}(s)$ and tangential $\mathbf{F}^t_{\alpha\beta}(s)$ analytical expressions for the forces between solid particles α and β are considered up to order $\mathcal{O}\left(1/\ln(s)\right)$, s being the distance between the surfaces of the spheres.

$$\begin{aligned} \mathbf{F}^n_{\alpha\beta}(s) &= f_{\alpha\beta}(s)\mathbf{V}_{\alpha\beta}\cdot\mathbf{e}_{\alpha\beta}\mathbf{e}_{\alpha\beta} \\ \mathbf{F}^t_{\alpha\beta}(s) &= g_{\alpha\beta}(s)\mathbf{V}_{\alpha\beta}\cdot\left(\mathbf{1}-\mathbf{e}_{\alpha\beta}\mathbf{e}_{\alpha\beta}\right) \end{aligned} \qquad (11)$$

where the scalar functions $f_{\alpha\beta}(s)$ and $g_{\alpha\beta}(s)$ are defined as

$$\begin{aligned} f_{\alpha\beta}(s) &= -6\pi\eta\left(\dot{\gamma}_{\alpha\beta}\right)\left[\frac{a^2}{4s} + \frac{9}{40}a\ln\left(\frac{a}{s}\right)\right] \\ g_{\alpha\beta}(s) &= -\pi\eta\left(\dot{\gamma}_{\alpha\beta}\right)a\ln\left(\frac{a}{s}\right) \end{aligned} \qquad (12)$$

for equal spheres of radius a. Both normal and tangential lubrication forces are applied for distances smaller than $s^n_c = r_{cut}/2$ and $s^t_c = r_{cut}/8$, which are the distances where the

estimations of the SPH model of the interaction force between spheres starts to fail due to lack of resolution [19, 26, 27].

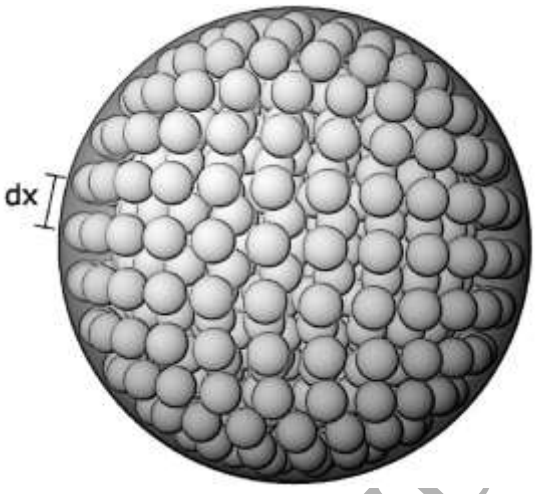

Fig. 6 Scheme of the location of the boundary particles (white spheres) within a solid sphere. The resolution is 5 particles per radius and corresponds to that used in this study.

The rheology of a complex solvent is included in Eqs. (11) through the functional dependence of the shear viscosity $\eta\left(\dot{\gamma}_{\alpha\beta}\right)$, where $\dot{\gamma}_{\alpha\beta}$ is the effective local shear rate between the solid suspended particles α and β. This can be estimated [1] as $\dot{\gamma}_{\alpha\beta} = 9\left|\mathbf{V}_{\alpha\beta}\right| / (16s)\sqrt{3a/s}$. The resulting lubrication dynamics in Eq. (11) are solved by an efficient implicit splitting scheme as discussed in detail in [24, 31].

Finally, additional repulsive forces between solid particles are introduced to prevent solid particle penetrability. They read [32, 33]

$$\mathbf{F}_{\alpha\beta}^{rep} = F_0 \frac{\tau e^{-\tau s}}{1-e^{\tau s}} \mathbf{e}_{\alpha\beta} \qquad (13)$$

where τ^{-1} determines the range of the repulsive force, and F_0 its magnitude. According to previous works [23] parameters chosen as $F_0 = 0.02115$ and $\tau^{-1} = 10^{-3}a$ allow us to model a hard-sphere interaction and prevent particle penetration.